Error localization examples: Looking for a needle in a haystack

L.G. Horta, [1] *M.C. Reaves,* [2] *and C.W. Fulcher* [3]

[1] Aerospace Engineer, NASA LaRC, lucas.g.horta@nasa.gov.
[2] Aerospace Engineer, NASA LaRC, mercedes.c.reaves@nasa.gov.
[3] Senior Engineer, Jacobs Engineering, NASA MSFC, clay.w.fulcher@nasa.gov

ABSTRACT

Finite element models (FEM) are routinely developed and used during fabrication of high dollar-value hardware. NASA, as part of the pre-flight certification of launch vehicles, routinely conducts vibration and static tests to calibrate models used for flight-risk assessments. During model calibration, certain areas of the model are modified, using engineering judgment and sensitivity analysis, to match the test results. Unfortunately, tools to identify problem areas in the FEM using test data directly are scarce and infrequently applied. Over the years, error localization algorithms have been proposed with very limited success. Recently, the Analytical Dynamics Model Improvement (ADMI) algorithm, which computes closed-form mass and stiffness corrections to match the test data exactly, have been shown to be an effective Error Localization Algorithm (ELA). The paper discusses three examples where ELA is used with simulated test data to locate problem areas. To gain confidence in the approach, the exact answer is shown along with ELA results. Results show that ELA is able to identify general problem areas consistent with known problem areas. In all examples, the ELA identified area is larger than the exact problem area. Nonetheless, with proper optimization tools, calibration results using the ELA identified areas provide excellent results.

1 INTRODUCTION

NASA and the aerospace industry routinely use Finite Element Models (FEM) to conduct analyses for risk assessments and flight readiness reviews. During the development of such models, contributions from many different areas are brought together to develop FEM, which are later validated and verified through carefully crafted tests. Because inputs from many engineers are integrated into the model at various stages of the hardware development, the task of model calibration, as defined in Refs. [1] - [4], often requires model developers to correct model deficiencies. Unfortunately, there is no universally accepted approach to identify problem areas in the FEM, which is particularly difficult with high-dimensional models. Often, analysts must correct model deficiencies with very little information about model flaws. Model adequacy is judged using established calibration metrics. For dynamic problems, calibration metrics are expressed in terms of frequency errors between test and analysis, cross orthogonality errors [5], and frequency response principal values [6]. To reconcile the model with test, the standard approach relies on engineering judgment, calibration metrics, sensitivity analysis, and energy analysis to decide what areas of the model to correct. Although these tools provide information about what is important in the model, this information is not necessarily related to problem areas in the model. Conventional metrics show the effects of model flaws as opposed to the causes. On the other hand, Error Localization Algorithms (ELA) are tools, which guided by test data, provide recommendations for model corrections. Hence, this is the focus of our work.

Although several ELA approaches have been proposed over the years, no particular approach have been adopted in commercial tools. Work here expands on the work in [7], which uses the Analytical Dynamics Model Improvements (ADMI) approach developed in [8]. The ADMI algorithm computes in closed-form, explicit mass and stiffness corrections to match test frequencies and mode shapes with analysis. Admittedly, many factors affect and even hinder our ability to compute model corrections. For example, the number of sensors, the number of modes, the quality of the measured data, and more importantly the fidelity of the nominal model are all extremely important factors. Nonetheless, under ideal conditions, ADMI can compute both mass and stiffness corrections exactly to reconcile model with test. Even under less than ideal conditions, ADMI can still provide model corrections, which can then be used to identify problem areas. The process of using ADMI results to connect to elements in the FEM is effectively the ELA process.

To gain confidence in the ability of the ELA process to identify problem areas, our work here presents three analytical examples: 1)a cantilever beam, 2)a tube, and 3) an isogrid panel. All three examples had their FEM perturbed to create simulated test data for use in the study. Degrees-of-freedoms (DOFS) affected by mass and stiffness corrections are mapped to elements, which are subsequently mapped to model properties. Results from applying ELA to each example are compared visually to known problem areas. Quantitatively, results are compared in terms of orthogonality values and frequency errors. Before showing the examples, a brief discussion of the model calibration process is presented.

2 MODEL CALIBRATION PROCESS

The model calibration process used with all examples starts with determining model areas in need of correction using the measured frequencies and mode shapes. Calibration starts with a reduced mass and stiffness from the nominal FEM, referred here as the Test Analysis Model (TAM). Because DOFS in the TAM connect the test data to potential problem areas in the model, TAM matrices should be as large as computationally possible to reduced loss of accuracy in the mass matrix. More importantly, TAM matrices are the basis from which corrections to the mass and stiffness are computed. DOFS or nodes affected by the corrections are mapped to FEM elements and subsequently to element properties. This process has been automated for FEM data decks generated using MSC Nastran [9] format.

Exact mass and stiffness corrections computed using ELA are difficult to implement through the physical FEM properties. Instead, corrections must be approximated using optimization tools. To implement corrections, the FEM is partitioned into zones according to the required changes. Specifically, the FEM bulk file is altered to have elements and properties renumbered according to zones. Once renumbered, any commercial model update tool can be used to conduct parameter updates. In our implementation, the MATLAB [10] optimization toolbox is used.

With the FEM bulk file altered, the next step is to solve for parameter values using optimization. The optimization strategy seeks to determine model parameters to reconcile the measured frequencies and modes shapes with the analysis. To accommodate both metrics, i.e., frequency and mode shapes, the objective function is defined in terms of a 2-norm

$$J = \left\| w_1 \Delta\lambda^T \gamma^T \gamma \Delta\lambda \quad w_2 tr(AA^T) \right\|_2 \tag{1}$$

The first scalar term in the objective function corresponds to the eigenvalue error defined as $\Delta\lambda^T = \begin{bmatrix} \omega_1^2 - \mu_1^2 & \omega_2^2 - \mu_2^2 & \dots & \omega_n^2 - \mu_n^2 \end{bmatrix}$, where ω_i are the predicted frequencies, μ_i are the measured frequencies, n is the total number of frequencies being reconciled, γ is a weighting vector for the individual frequencies, and w_1 is a user-prescribed scalar to adjust the objective function scaling. To apply Eq. 1, test and analysis frequencies must be paired first using orthogonality. Pairing links a test mode to an analysis mode when the cross-orthogonality value is above a user-prescribed threshold.

The second scalar term in Eq. 1 is the orthogonality error computed using the trace $tr(AA^T)$,where $A = \Phi^T M \Psi - I$. This calculation includes the measured modes shapes Φ, the analysis mode shapes Ψ, a reduced mass matrix M, an identity matrix I, and an arbitrary user-prescribed scalar w_2 to adjust the objective function scaling. Close-form expressions for the gradient have been developed and used.

3 ERROR LOCALIZATION EXAMPLES

To understand the capabilities and limitations of ELA, it is best to use examples where problem areas are known. For this purpose,

three examples are discussed where FEM alterations are implemented to create simulated test data. Data in terms of frequencies and mode shapes from the altered models are used to identify problem areas. Because the altered locations are known, results from ELA are easily verified qualitatively.

3.1 Cantilever Beam

Our first example is a beam, shown in Fig. 1, with translations constrained at both ends and no longitudinal rotations. Ten bar elements with rectangular cross-sections are used to construct the model. Heretofore, the term test data is used to refer to simulated mode shapes and frequencies from a perturbed FEM. Test shapes contain displacements at 9 locations in the lateral (y) and vertical (z) directions. In this example, the perturbed FEM has the cross-section height, in the area labeled $Mod\ 1$, changed from 0.125 to 0.150, and the width in the area of $Mod\ 2$ reduced from 1.0 to 0.8 inches.

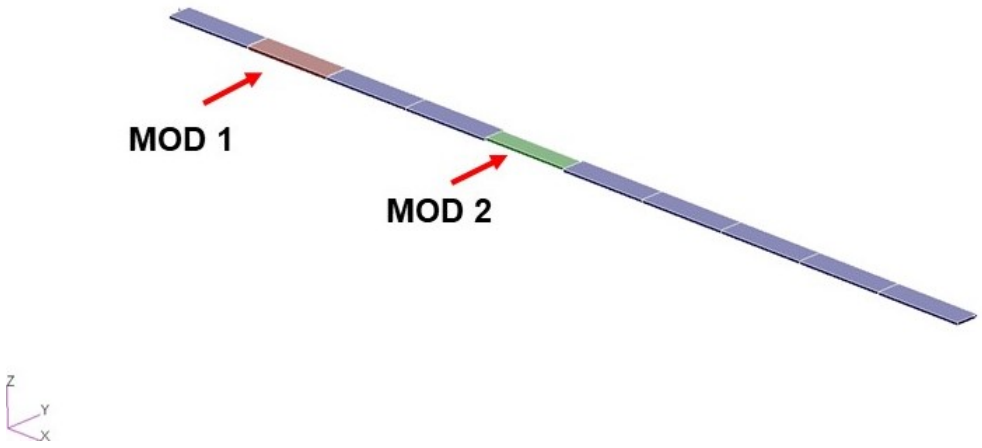


Figure 1: Beam model

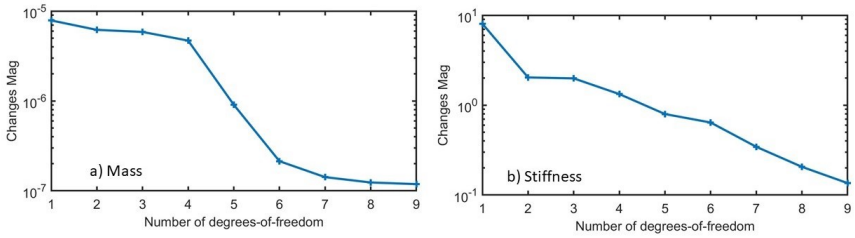


Figure 2: Error localization computed changes for a) mass and b) stiffness

Starting with TAM matrices sized 27 x 27, six test modes are used with ELA to compute mass and stiffness changes to match the test data. ELA results in Fig. 2a, shows the sorted mass changes and Fig. 2b shows the sorted stiffness changes a function of the number of degrees of freedom changed. In here, the number of degrees of freedom refer to the number of changes as a function of diagonal elements in ΔM and ΔK to produce the necessary change. After reviewing the mass changes, it should be apparent that only four DOFS show the largest change. However, stiffness changes include many more DOFS.

When computing ELA corrections, the ability to correct a model depends on many factors. It is critical that TAM mode shapes

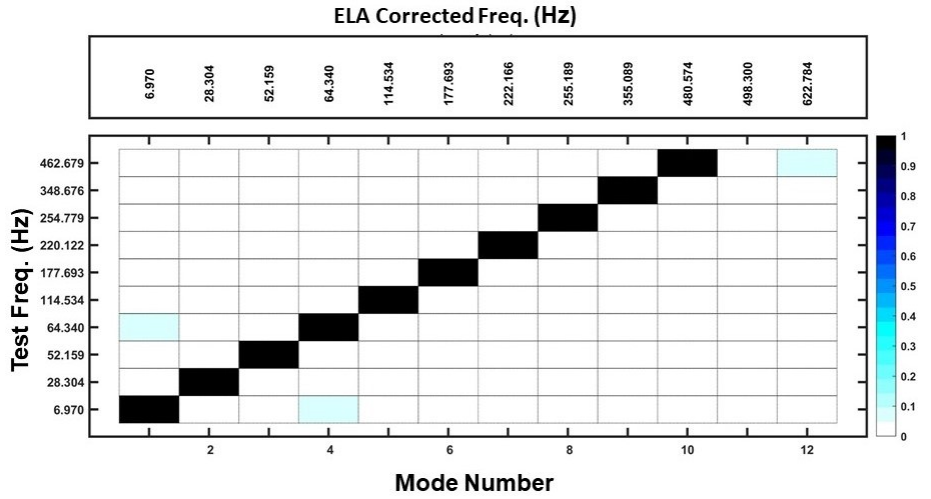


Figure 3: Cross-orthogonality between test and ELA corrected model

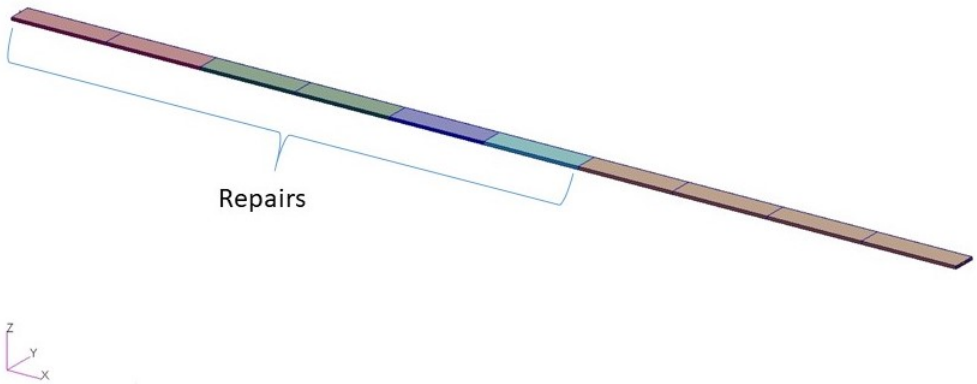


Figure 4: Beam repair areas identified using ELA

span the vector space of the measured modes. Cross-orthogonality (CO) results (i.e. triple product $\Phi^T M \Psi$) between test data (ordinate) and the corrected model (abscissa), shown in Fig. 3, are a way to verify the adequacy of the ELA solution. CO values of 1 are shown in black. Note that the first six modes are matched exactly, as evident when comparing test and corrected model frequencies. A corrected ELA model is simply the TAM model with corrections; i.e.,$M + \Delta M$ and $K + \Delta K$. These matrices are not necessarily realizable through the FEM parameters. FEM parameter changes to approximate the corrected ELA solution must be implemented using numerical optimization.

Implementation of model changes begins by linking DOFS identified by ELA to elements and properties in the FEM. Figure 4 shows such a link among the FEM elements and locations in need of corrections. Six bar elements, marked using different colors, must be repaired based on ELA corrections. With elements identified, users must still chose among a large number of parameters for calibration. Table 1 list 16 parameters for the repaired area; comprised of 4 parameters per bar element.

To set up the optimization problem, weights for the first six test modes are prescribed as $\gamma^T = \left[{}^{10}/_{\mu_1^2} \quad {}^{10}/_{\mu_2^2} \quad {}^{10}/_{\mu_3^2} \quad {}^{1}/_{\mu_4^2} \quad {}^{1}/_{\mu_5^2} \quad {}^{1}/_{\mu_6^2} \right]$ and the objective function weights are set to $w_1 = 10$ and $w_2 = 10$. Parameter sensitivities are computed using Solution 200 in MSC Nastran [9] while mode shape derivatives are computed using Nelson's Method

[11]. A gradient-based optimization algorithm is linked to MSC Solution 200 for optimization. After 148 iterations, the optimizer found the solution listed in Table 1 under $Cal.\ Value$. Of the 16 parameters, only 7 show appreciable changes within four significant digits. Table 2 compares frequencies for the perturbed, nominal, and calibrated model. Note that frequency errors for the calibrated model are all within 0.64%. In addition, Cross-orthogonality (CO) results are compared in Fig. 5; test (ordinate) versus nominal (abscissa) is shown in Fig. 5a and test versus calibrated model is shown in Fig. 5b; off-diagonal values are all within 5% for the calibrated model. A good rule-of-thumb is to have CO diagonal values near 1 and off-diagonal values less than 5%. Finally, because geometrical parameters are adjusted, it is worth noting that the total mass after calibration increased from 0.5008 lbs to 0.5010 lbs. If one needs to maintain a fixed mass, mass can be included as an additional constraint.

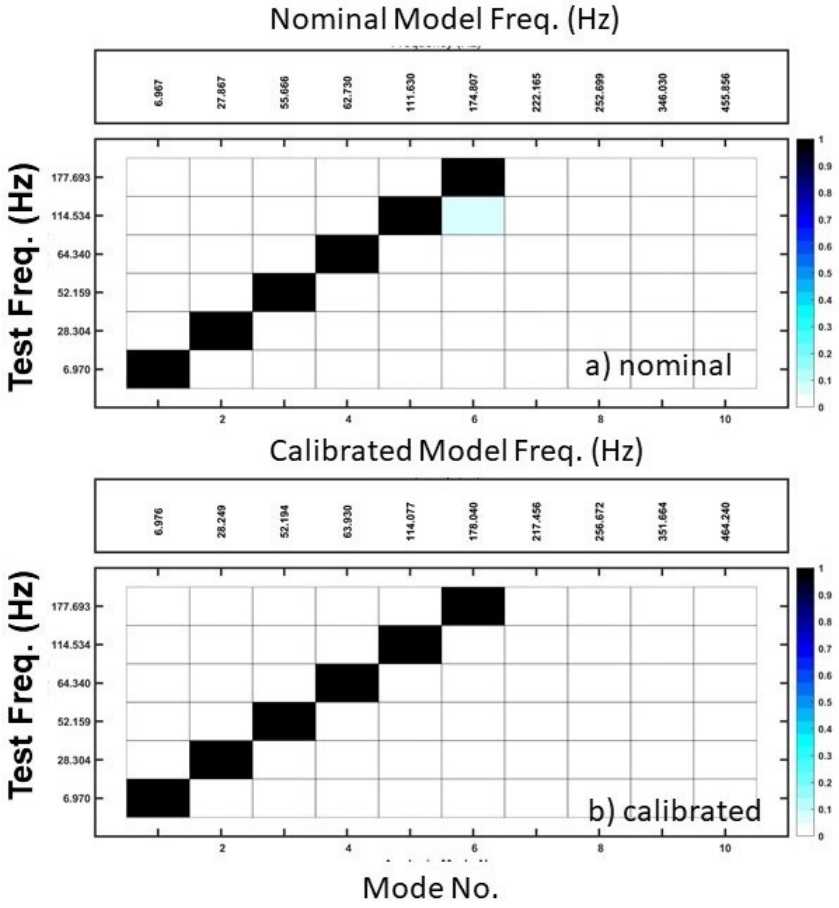


Figure 5: Cross-orthogonality for: a) test versus nominal, b) test versus calibrated

3.2 Cantilever Tube

The second example shown in Fig. 6 is a cantilever tube 36 inches long with diameter of 2 inches; modeled with 1589 grid points and 768 CQUAD elements. For this study optimal sensor placement, conducted as part of the pretest analysis, selected 209 locations; marked with green arrows in Fig. 6. Optimal sensor placement is extremely important to ensure that modes are distinguishable from each other. Table 3 list the first 8 frequencies of the perturbed, nominal, and calibrated models. The perturbed FEM is created by altering the region indicated with magenta arrows in Fig. 6. Eight test modes, from the perturbed model, are used to locate errors using ELA. After applying ELA, results produced mass corrections as shown in Fig. 7a and stiffness corrections as shown in Fig. 7b. The ordinate in Fig. 7a and 7b shows the magnitude of diagonal elements in ΔM and ΔK, respectively, sorted in descending order as a function of number of DOFS. Note that mass corrections are very small, with the largest changes between 6.86×10^{-9} and 1.8×10^{-9} , encompassing only 33 DOFS. In contrast, stiffness corrections are significant and affect a large number of DOFS.

TABLE 1: Beam calibration parameters

Par No.	Zone ID	Units	Nominal Value	Label	Cal. Value
1	555001	in^2	0.1250	A	0.1179
2	1110001	in^2	0.1250	A	0.1248
3	1665001	in^2	0.1250	A	0.1250
4	2220001	in^2	0.1250	A	0.1435
5	555001	in^3	0.0002	I1	0.0002
6	1110001	in^3	0.0002	I1	0.0002
7	1665001	in^3	0.0002	I1	0.0002
8	2220001	in^3	0.0002	I1	0.0002
9	555001	in^3	0.0104	I2	0.0083
10	1110001	in^3	0.0104	I2	0.0104
11	1665001	in^3	0.0104	I2	0.0083
12	2220001	in^3	0.0104	I2	0.0083
13	555001	in^3	0.0006	J	0.0006
14	1110001	in^3	0.0006	J	0.0006
15	1665001	in^3	0.0006	J	0.0006
16	2220001	in^3	0.0006	J	0.0006

TABLE 2: Beam frequencies for nominal, perturbed, and calibrated model

Par. No.	Pert. Freq. (Hz)	Nom. Freq. (Hz)	Nom. Freq. Error (%)	Cal. Freq. (Hz)	Cal. Freq. Error (%)
1	6.97	6.967	-0.04	6.976	0.09
2	28.304	27.867	-1.54	28.249	-0.19
3	52.159	55.666	6.72	52.194	0.07
4	64.340	62.730	-2.50	63.930	-0.64
5	114.534	111.630	-2.54	114.077	-0.40
6	177.693	174.807	-1.62	178.04	0.20

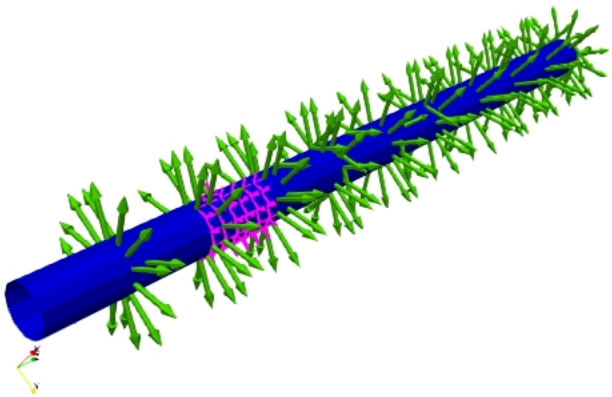


Figure 6: Tube sketch with sensor placement (green-arrows) and damaged area (magenta arrows)

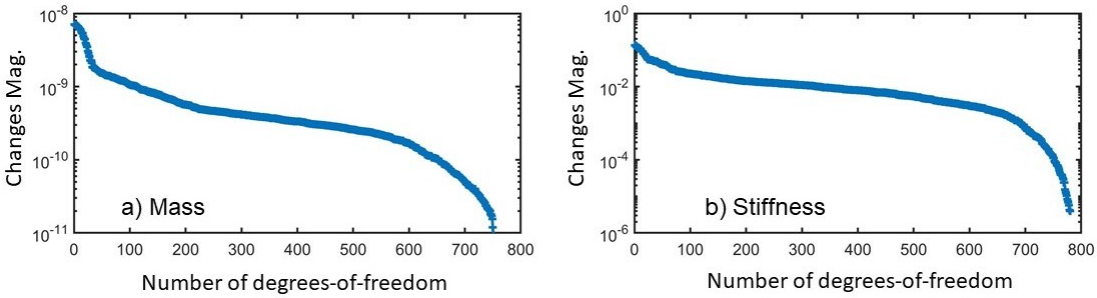


Figure 7: Error localization computed changes for a) mass and b) stiffness

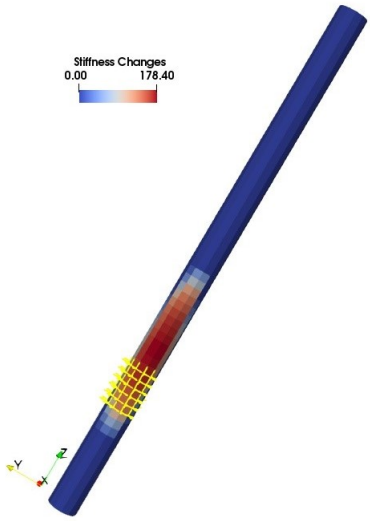


Figure 8: Mapping of ELA stiffness corrections onto elements in the FEM

Because mass corrections are small, model repairs map only stiffness DOFS identified by ELA onto elements in the FEM. Figure 8 shows ELA element mapping using color shading. Superimposed onto the tube in yellow is the perturbed area. Note that the known perturbed area is within the stiffness changes recommended by ELA. As mentioned earlier, ELA corrections are not linked to physical parameters in the FEM. In order to connect ELA corrections to physical parameters, the FEM must be partitioned and elements renumbered according to ELA. Because of the large number of model changes required, the process is automated and the partitioned FEM along with renumbered properties are created and stored in a separate file. In this example, the partitioned FEM contains 123 zones, as shown in Fig. 8. To adjust stiffness values in the zones, the modulus is used in the optimization process to reconcile the model with test.

Ideally, one would like to change physical parameters to match the computed ELA corrections exactly. Unfortunately, this problem is very difficult and can only be approximated using numerical optimization. In this example, the optimization starts by prescribing test frequencies weights $\gamma^T = 10\left[1/\mu_1^2 \quad 1/\mu_2^2 \quad \cdots \quad 1/\mu_8^2\right]$ and objective function weights as $w_1 = 1$ and $w_2 = 0.1$. As with the first example, a gradient based optimization algorithm is used to reconcile model with test. After 48 iterations, the optimizer converged and the calibrated model frequencies are shown in Table 3 under Cal-1; frequency errors less than 0.2%.

At this point, it is educational to compare calibration solutions when using ELA versus a standard approach where zoning is based on engineering judgement and sensitivity. For that purpose, the tube model is also calibrated using standard zoning and ATA Engineering

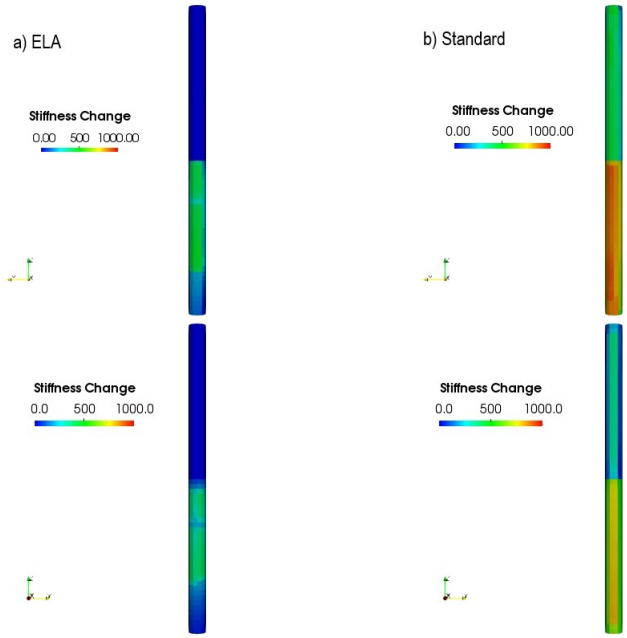


Figure 9: Calibrated model changes using a) ELA zoning, and b) Standard sensitivity information

Attune Software [13] and [14]. Frequencies, when using the calibrated parameters and standard zoning are shown in Table 3 under Cal-2. Note that frequency matching is excellent with errors under 1%. When comparing frequencies between calibrated models, it is not apparent that the actual stiffness changes with each approach are drastically different. A way to examine these two calibrated models is to compare the actual stiffness changes produced by each solution. Figure 9a shows contour plots of Cal-1 stiffness changes when using ELA zoning (front-view top, back-view at the bottom) and Fig. 9b shows Cal-2 stiffness changes when using the standard zoning approach. Clearly, not only the stiffness changes are dramatically different but also the affected regions. More importantly, ELA changes are concentrated near the known problem area, whereas the standard approach produced changes over the entire tube.

Fig. 10a shows CO results for test (ordinate) versus Cal-1 (abscissa), whereas Fig. 10b shows test versus Cal-2. CO off-diagonal values for Cal-1 are all within 5% for the calibrated model, whereas for Cal-2 some values are about 10%. High Cal-2 CO errors after calibration with Attune simply indicate that the solution has not converged and additional iterations are needed.

TABLE 3: Tube frequencies for perturbed, nominal, and calibrated models

Mode No.	Pert. Freq. (Hz)	Nom. Freq. (Hz)	Nom. Freq. Error (%)	Cal-1 Freq. (Hz)	Cal-1 Error (%)	Cal-2 Freq. (Hz)	Cal-2 Error (%)
1	53.8	54.4	1.0	53.8	-0.1	53.7	-0.3
2	58.6	61.1	4.1	58.7	0.2	59.1	0.8
3	334.0	332.6	-0.4	333.2	-0.2	334.5	0.1
4	368.6	367.1	-0.4	367.8	-0.2	366.7	-0.5
5	527.6	529.0	0.3	527.9	0.1	532.8	1.0
6	536.8	538.5	0.3	537.1	0.0	535.0	-0.3
7	543.1	546.9	0.7	543.6	0.1	543.7	0.1
8	551.5	555.8	0.8	551.9	0.1	547.2	-0.8

3.3 Isogrid panel

The third example discussed here is motivated by a study conducted at NASA Langley to evaluate the adequacy of using equivalent panel properties, derived from static approximations, to model the dynamic behavior of isogrid panels. Figure 11 shows on the left a picture of a rectangular isogrid panel 8 x 14 1/8 x 3/32 inches weighting 1.35lbf. For small panels, modeling the complex pattern of the ribs is not difficult but for large panels, the computational complexity is often large. In 1973, the McDonald Douglas Astronautics Company under contract for NASA [12] developed a computational handbook with formulas to estimate the equivalent properties for isogrid designs to approximate their static behavior. On the right of Fig. 11 is a sketch of the FEM, hereafter referred to as the Panel-Equivalent Model (PaEM), developed using equivalent isogrid properties. As before, simulated test data are created by perturbing the FEM. Specifically, the perturbed FEM has an edge added along the border. For ELA evaluation, test data are collected at the 23 locations shown with arrows in Fig. 11.

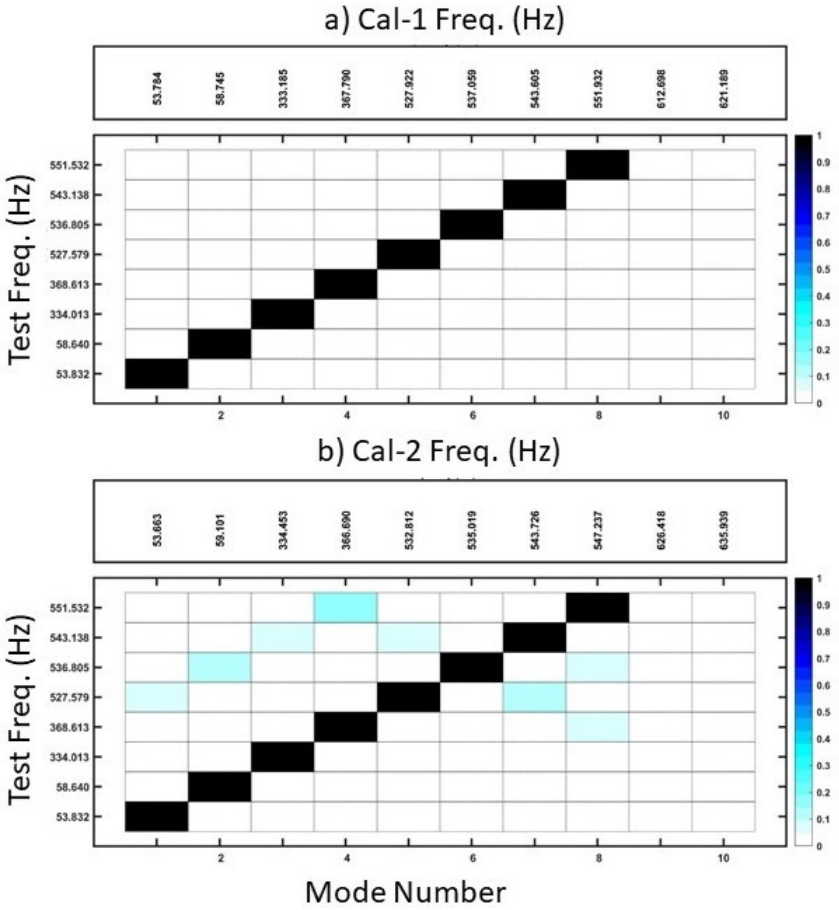


Figure 10: Tube cross-orthogonality of calibrated model when using a) ELA zoning and b) Standard zoning

Although the panel geometry is relatively simple, the panel itself has a slight curvature, which makes the modeling effort somewhat more difficult. The PaEM, modeled with MSC Nastran while suspended from soft strings, has 496 nodes (2976 DOFS) and 450 CQUAD4 elements. Panel layers (i.e., skin and ribs) are modeled using composite laminate theory with isotropic properties for the skin and isogrid properties for the rib; properties computed using the isogrid design formulas [12]. Table 4 list the first 6 modal frequencies excluding low frequency pendulum modes.

To implement the ELA, a TAM model for the PaEM is created with 1488 DOFS. TAM pendulum modes are shifted outside the frequency range of interest in this study. The first 6 test modes, all perturbed modes, are used in ELA to compute mass and stiffness corrections that reconcile the test frequencies and mode shapes with the analysis. Figure 12 shows mass and stiffness corrections,

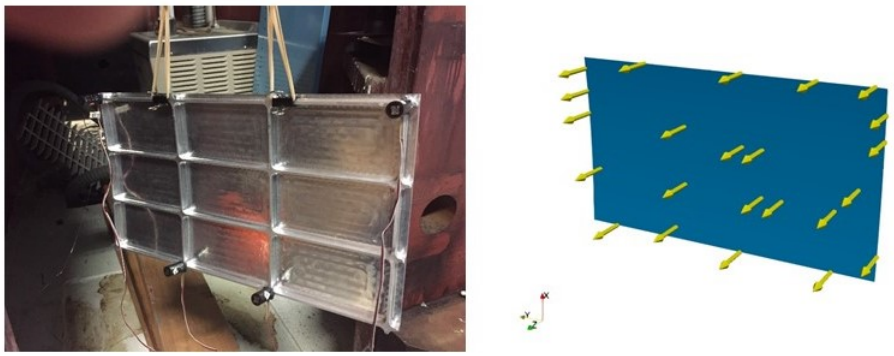


Figure 11: Isogrid panel (left) and FEM sensor placement (right)

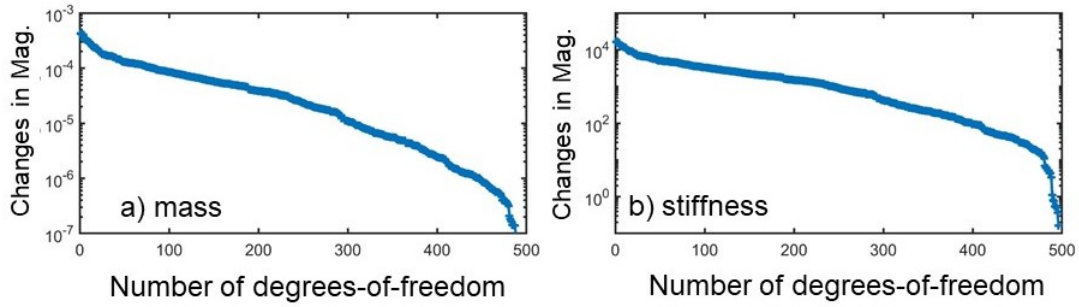


Figure 12: Sorted ELA corrections to repair 6 modes of the nominal model for a) mass, and b) stiffness as a function of the number of degrees of freedom

sorted in descending order, as a function of the number of DOFS. Of importance is the relative magnitude of the necessary changes to correct the model. If the magnitudes are large, this can be a reflection of either bad test data, inadequacy of sensor placement, or a poorly constructed model. Linking of the affected DOFS (or nodes) to elements in the FEM is what provides users with a more intuitive picture of problem areas. Figure 13 shows a contour plot of ELA stiffness changes needed to reconcile the model. Also shown is the FEM perturbed area marked with green arrows. Note that most of the perturbed area overlaps the ELA corrections but not all. The number of sensors and number of modes have a significant impact on our ability to identify problem areas, and in this example, only 23 sensors and 6 modes are used.

A more difficult task is to map ELA corrections to physical parameters. For this, the FEM is partitioned into 123 zones. After extracting parameters for the 123 zones, the material modulus is optimized to reconcile the model with test.

To begin the optimization process, test frequencies weights are set to $\gamma^T = \begin{bmatrix} 1/\mu_1^2 & 1/\mu_2^2 & \cdots & 1/\mu_6^2 \end{bmatrix}$ and the objective function weights are $w_1 = 100$ and $w_2 = 1$. As before, a gradient-based optimization algorithm is used to reconcile the model with test. After 40 iterations, the optimizer converged and the calibrated model frequencies, shown in Table 4 under calibrated model, show that frequency errors have been reduced to less than 1.2%. Moreover, actual stiffness changes with the calibrated model are shown in Fig. 14. In this problem, only the modulus of the material has been changed and therefore the system mass is constant. Clearly, the optimization process is intended to reproduce the stiffness changes shown Fig. 13. To seek a closer solution, users can select other parameters within the 123 zones (like thickness, moments of inertia, etc) for optimization. Nonetheless, in spite of the obvious differences between ELA and the calibrated model stiffness, frequencies errors are relatively small.

Finally, results for the CO are shown in Fig. 15. As before, color shading correspond to CO values between 0 and 1. Standard

TABLE 4: Panel equivalent model frequencies

Mode No.	Pert. Freq. (Hz)	Nom. Freq. (Hz)	Nom. Freq. Error (%)	Cal. Freq. (Hz)	Cal. Error (%)
1	114.5	107.7	-5.94	115.2	0.61
2	378.2	359.2	-5.02	382.5	1.14
3	437.8	392.5	-10.35	434.9	-0.66
4	792.0	767.8	-3.06	798.0	0.76
5	881.3	795.7	-9.71	874.7	-0.75
6	992.0	953.9	-3.84	994.8	0.28

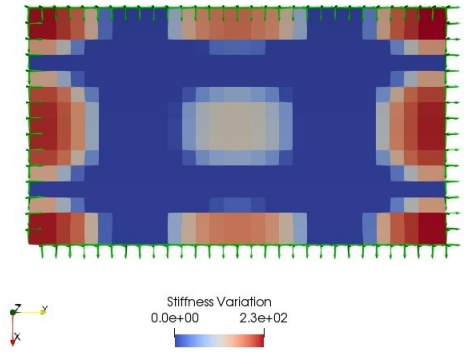


Figure 13: Computed stiffness corrections using ELA; green arrows correspond to the known perturbations

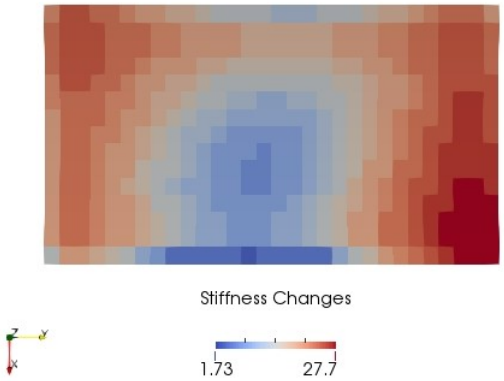


Figure 14: Stiffness changes when using calibrated parameters

practices often recommends CO off-diagonal values be less than 5%. Figure 15a shows that off-diagonal values for the nominal and calibrated models are less than 30%. Improvements from calibration are primarily associated with the frequencies and mode 6 alignment. Large errors in the CO off-diagonal are mainly due to a small sensor count.

As should be evident by these three example problems, the ELA method is able to identify problem areas in the model when provided with adequate test mode shapes and frequencies. Nonetheless, readers are reminded that there are many factors that affect our

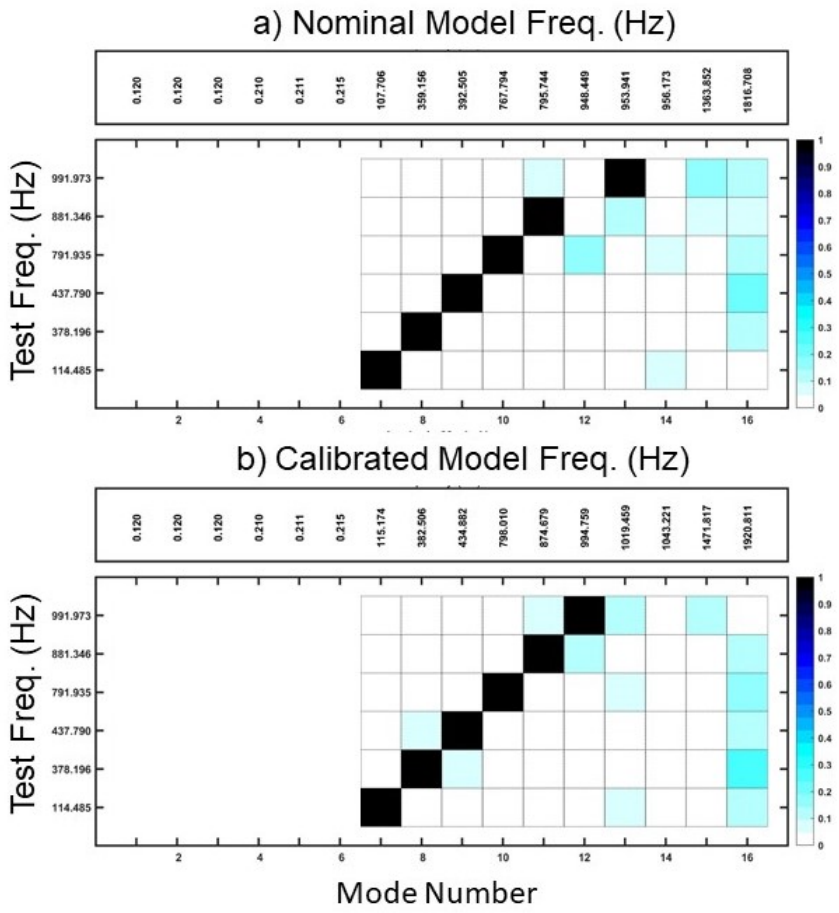


Figure 15: Cross orthogonality between a) test versus nominal model, and b) test versus calibrated model

ability to determine problem areas in the FEM. For example, poorly planned tests, improper sensor placement, missing modes, and inadequate FEM models are among the most critical. Until now, users have never been able to use test data directly to identify problem areas in the model. From the perspective of a user, finding model flaws is like finding a needle in a haystack.

4 CONCLUSIONS

The objective of this paper is to discuss the application of an Error Localization Algorithm (ELA) to identify problem areas in a Finite Element Model using modal test data. Three examples are presented to demonstrate the ability of the ELA approach to identify repair areas in the model. ELA determines numerical mass and stiffness corrections, which point to problem areas in the model. Although ELA corrections are not linked directly to parameter changes, the link is established using numerical optimization. The paper shows that ELA is able to identify general problem areas consistent with known problems. More importantly, using the identified areas, models are reconciled successfully. In general, the identified areas are larger than the exact answer.

Results from comparing stiffness changes using ELA versus a standard approach revealed that although model calibration, in terms of mode and frequency matching, is certainly possible with more heuristic approaches, changes in the stiffness between the two approaches can be drastically different. Without the benefit of knowing what areas to correct, the only option is to adjust everything because commercial model update tools rely exclusively on sensitivity to implement model changes. ELA can now provide a new capability to better localize update areas.

REFERENCES

[1] Friswell, M.I, and Mottershead, J.E. Finite Element Model Updating in Structural Dynamics. *Copyright Kluwer Academic Publisher*, Reprinted 1996, ISBN 0-7923-3431-0 (1995)

[2] Maia, N.M.M, Silva, J.M.M, He, J., Lieven, N.A.J, Lin, R.M., Skingle, G.W., To, W-M, and Urgueira, A.P.V. Theoretical and Experimental Modal Analysis. *Research Studies Press LTD*, ISBN 0-471-97067-0 (1997)

[3] Anonymous. Guide for the Verification and Validation of Computational Fluid Dynamics Simulations. *AIAA*, G-077-1998 (1998)

[4] Anonymous. Guide for Verification and Validation in Computational Solid Mechanics. *ASME*, Verification and Validation 10-2006 (2006)

[5] Blelloch, P.A., and Vold, H. Orthogonality of large models - What's the Problem. *Proceedings of the 23rd International Modal Analysis Conference (IMAC)* (2005)

[6] Horta, L.G., Reaves, M.C., Buehrle, R.D., Templeton, J.D., Lazor, D.R, Gaspar, J.L., Parks, R.A., Bartolotta, P.A. Finite Element Model calibration for Ares I-X Flight Vehicle. *Journal of Engineering Mechanics*, DOI 10.1001/s11340-010-9456-x (2011)

[7] Horta, L.G., and Reaves, M.C. An implementation of error localization algorithms for model calibration of dynamical systems. *SN Applied Sciences (2020)* 2:1027, Published on-line 06 May 2020, https://doi.org/10.1007/s42452-020-2744-x

[8] Wei, F-S. Analytical dynamic model improvement using vibration test data. *AIAA Journal*, Vol. 28, pp. 175-177 (1990)

[9] Anonymous. MSC Nastran multidisciplinary structural analysis. The MacNeal-Schwendler Corporation, https://www.msc.software.com (2019)

[10] Anonymous. MATLAB R-2018B, Copyright 1994-2019, The Mathworks Inc. *http://www.mathworks.com* (2018)

[11] Nelson, R.B. Simplified Calculation of Eigenvector Derivatives. *AIAA Journal*, Vol. 14, No. 9, (1976)

[12] Anonymous. Isogrid Design Handbook. Prepared by McDonnel Douglas Astronautics Company, MDC-G4295A, Contract NAS 8-28619, Revised April 2004. (1973)

[13] IMAT *http://www.ata-e.com/software/imat*

[14] ATTUNE *http://www.ata-e.com/software/attune*